Iridium-Hydride-Mediated Stannane–Fluorine and –Chlorine sigma-Bond Activation: Reversible Switching between X-type Stannyl and Z-type Stannane Ligands

Iridium-Hydride-Mediated Stannane−Fluorine and −Chlorine σ-Bond Activation: Reversible Switching between X-type Stannyl and Z-type Stannane Ligands

Hajime Kameo,*[,†] Yuki Baba,[†] Shigeyoshi Sakaki,[‡] Didier Bourissou,[§,‖] Hiroshi Nakazawa,[⊥] Hiroyuki Matsuzaka[†]

[†] Department of Chemistry, Graduate School of Science, Osaka Prefecture University, Gakuen-cho 1-1, Naka-ku, Sakai, Osaka 599-8531, Japan

[‡]Fukui Institute for Fundamental Chemistry, Kyoto University, Takano-nishihiraki-cho 34-4, Sakyo-ku, Kyoto 606-8103, Japan

[§] Université de Toulouse, UPS, Laboratoire Hétérochimie Fondamentale Appliquée, 118 route de Narbonne, F-31062 Toulouse, France

[‖] CNRS, LHFA UMR 5069, F-31062 Toulouse, France

[⊥] Department of Chemistry, Graduate School of Science, Osaka City University, Sugimoto 3-3-138, Sumiyoshi-ku, Osaka 558-8585, Japan

ABSTRACT

The Iridium(I) carbonyl hydride Ir(H)(CO)(PPh_3)$_3$ (**1**) cleaves the Sn−F and Sn−Cl bonds of the four-coordinate stannanes {*o*-(Ph_2P)C_6H_4}$_3$Sn(X) (X = F (**2a**), Cl(**2b**)) to afford the stannyl complex [{*o*-(Ph_2P)C_6H_4}$_3$Sn]Ir(CO) (**3**) and HX (X = F, Cl) thanks to phosphine chelation. A plausible intermediate [{*o*-(Ph_2P)C_6H_4}$_3$(Cl)Sn]Ir(H)(CO) (**6**) featuring Z-type Ir→R_3SnCl interaction was synthesized by the reaction of **3** with HCl. Compound **6** readily regenerated **3** upon treatment with Brønsted bases, enabling reversible switching between X-type stannyl and Z-type stannane ligands. DFT calculations suggest plausible pathways for Sn−F and Sn−Cl bond cleavage reactions, and support that the species bearing a Z-type Ir→R_3SnX interactions (X = F, Cl) are intermediates for Sn−X bond cleavage.

INTRODUCTION

Transition metal-mediated bond activation participates in a range of catalytic systems,[1] and therefore the study of bond activation by transition metals is essential for opening the possibility of novel catalytic reactions. Heavier group 14 elements such as silicon and germanium form a polar and considerably strong σ-bonds with fluorine,[2,3] and the E−F σ-bonds (E = Si, Ge) in four-coordinate silanes and germanes are rarely activated by transition metals.[4] Tin also makes very strong σ-bond with a fluoride,[3] however it is known that early transition metal complexes can cleave not only Sn−F σ-bonds in hypervalent species but also Sn−F σ-bonds in four-coordinate stannanes.[5,6] Roesky et al. reported that Cl/F exchange effectively occurs in reactions between Me_3SnF and early transition metal chloride species.[6,7] For example, titanocene chloride dimer $[(Cp_2Ti)(\mu\text{-}Cl)]_2$ reacts with Me_3SnF to afford the fluoride analogue $[(Cp_2Ti)(\mu\text{-}F)]_2$ and Me_3SnCl (Scheme 1a).[6a] On the other hand, late transition metal complexes rarely cleave Sn−F bond of four-coordinate stannanes. This is probably attributed to high affinity between relatively electropositive early transition metals and fluorine, the most electronegative element. Actually, the Cl/F exchange is thermodynamically feasible in titanocene chloride dimer (ΔG^0_{298K} = −7.1

kcal/mol), while Cl/F exchange in Vaska type complex is endergonic (ΔG^0_{298K} = 7.8 kcal/mol).[8] For the development of Sn−F activation by late transition metals, a new method besides Cl/F exchange is required. Holland et al. achieved reductive Sn−F bond cleavage through a radical pathway (Scheme 1b), in which a cobalt(I) complex cleaved the Sn−F bond in Me_3SnF to afford a doubly-bridged fluoride cobalt(II) complex accompanied with the formation of several stannanes bearing Sn−Sn bonds.[9]

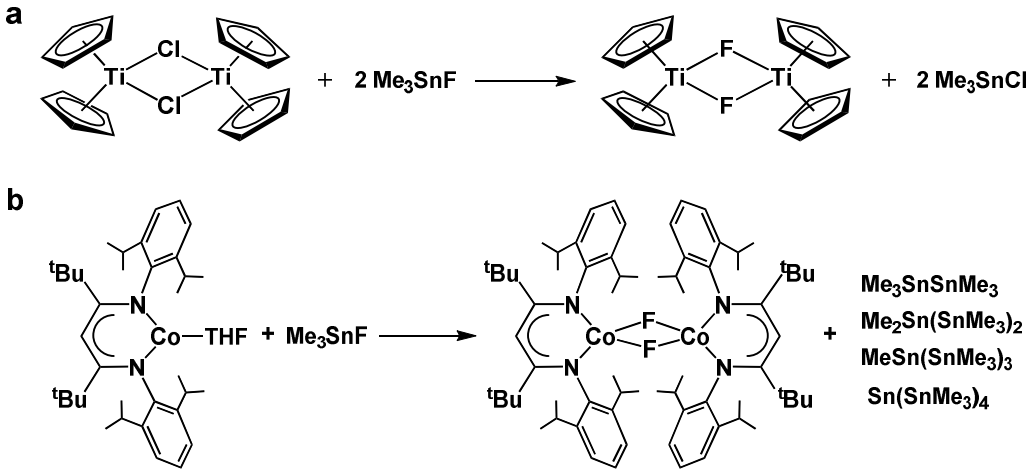

Scheme 1. (a) Cl/F exchange reaction of $[(Cp_2Ti)(\mu\text{-}Cl)]_2$ with Me_3SnF.[6a] (b) Reductive Sn−F bond cleavage via a radical pathway by the cobalt(I) complex.[9]

Recently, we reported iridium-hydride-mediated bond activation reactions using phosphine chelation.[10] The cleavage of Si−F bonds[10c] in $\{o\text{-}(Ph_2P)C_6H_4\}_2Si(F)_2$ and

{*o*-(Ph_2P)C_6H_4}$_3$Si(F) as well as Ge−F bond[10d] in {*o*-(Ph_2P)C_6H_4}$_2$Ge(F_2 were achieved by the reactions with the iridium hydride Ir(H)(CO)(PPh_3)$_3$ (**1**) (Scheme 2) through σ-bond metathesis involving Ir−H and E−F bonds (E = Si, Ge) (Figure 1a). The chelation strategy also facilitates the cleavage of Si−Cl and Ge−Cl bonds in chloro analogues {*o*-(Ph_2P)C_6H_4}$_2$E(Cl_2 (E = Si, Ge) by **1**, in which S_N2-type pathway was proposed (Figure 1b).[10e] These findings prompted us to investigate the activation of Sn−F and Sn−Cl bonds. We herein report iridium-mediated Sn−F and Sn−Cl bond activation together with mechanistic studies using DFT calculations. Further, interconversion between Z-type (2 electron acceptor)[11] stannane and X-type stannyl coordination is substantiated.

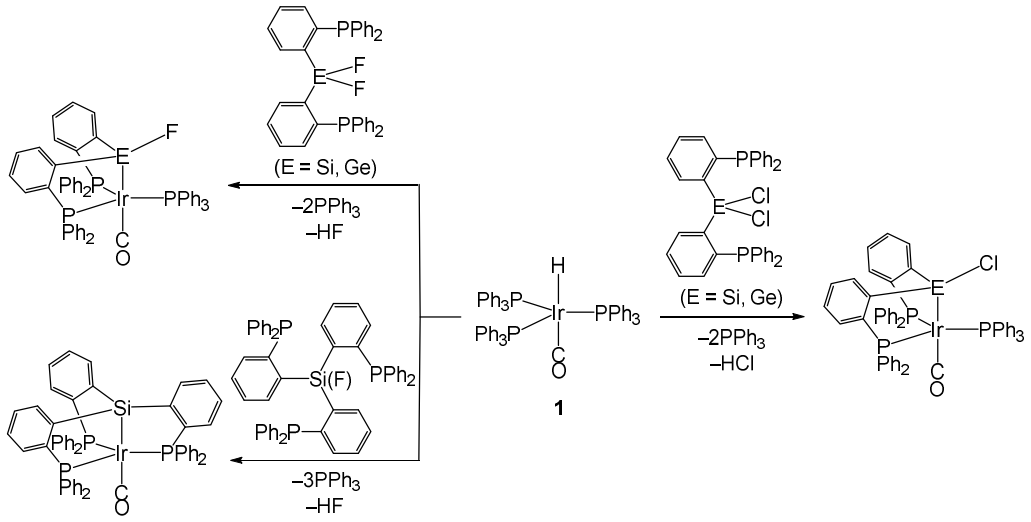

Scheme 2. Si−F σ-bond cleavages of {*o*-(Ph_2P)C_6H_4}$_n$Si(F)$_{(4-n)}$ (n = 2, 3)[10c] and Ge−F σ-bond cleavage of {*o*-(Ph_2P)C_6H_4}$_2$Ge(F_2[10d] by iridium hydride **1**.

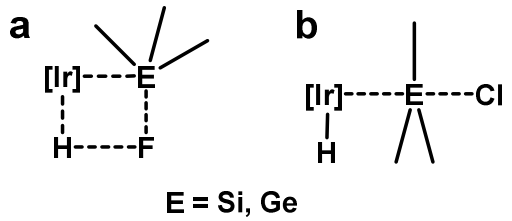

Figure 1. (a) σ-bond metathesis for Si−F and Ge−F σ-bond cleavage. (b) S_N2-type reaction for Si−Cl and Ge−Cl σ-bond cleavage.

RESULTS AND DISCUSSION

To investigate the possibility of Sn−F bond cleavage by **1**, we attempted to synthesize P_2SnF_2-type compound $\{o\text{-}(Ph_2P)C_6H_4\}_2Sn(F)_2$. However, the synthesis of this precursor was unsuccessful despite of a lot of efforts. Therefore we employed the P_3SnF-type compound $\{o\text{-}(Ph_2P)C_6H_4\}_3Sn(F)$[12] (**2a**) (Scheme 3). Reaction of iridium hydride **1** with **2a** took place over 60 °C, and the reaction was completed at 80°C within 32 hours to afford a mixture of $[\{o\text{-}(Ph_2P)C_6H_4\}_3Sn]Ir(CO)$ (**3**)[13] and $[\{o\text{-}(Ph_2P)C_6H_4\}_2(F)Sn]Ir(CO)(PPh_3)$ (**4a**) in a ratio of 41:59.[14] Product **3** was produced through the expected Sn−F bond activation, while **4a** was probably formed through the oxidative addition of $Sn-C_{Ar}$ bond[15] of **2a** followed by the reductive elimination of the $H-C_{Ar}$ bond (Scheme 4). Although one may expect that the Sn−C bond in **3** is cleaved by HF, the Sn−C bond remained unchanged in

the reactions of **3** with HF·pyridine and K[HF_2] (vide infra). Similar types of Sn-C bond cleavages were reported by our group[10a] and Iwasawa et al,[16] and in this study the feasibility of the Sn−C_{Ar} bond cleavage was ascertained by DFT calculations (see page S21 in Supporting Information). Although the formation of HF and HF_2^- could not be confirmed by ^{1}H and ^{19}F NMR spectroscopy, ^{19}F and ^{31}P NMR spectra indicated the formation of several intractable products, which were the same as the products from the reaction of PPh_3 with K[HF_2]. Therefore, it is likely that PPh_3 acts as a scavenger of HF in a similar way to Si−F and Ge−F bond cleavage reactions by **1**.[10c,10d]

Next, Sn−Cl bond activation was investigated by using the P_3SnCl-type precursor {*o*-(Ph_2P)C_6H_4}$_3$Sn(Cl) (**2b**).[17] The reaction of **1** with **2b** took place under similar conditions to those of the reaction with **2a** to afford a mixture of Sn−Cl and Sn−C_{Ar} cleaved products **3** and [{*o*-(Ph_2P)C_6H_4}$_2$(Cl)Sn]Ir(CO)(PPh_3) (**4b**) in a ratio of 70:30 (Scheme 3).[14] Although HCl was not detected by ^{1}H NMR spectroscopy, ^{31}P NMR measurements supported the formation of phosphonium [$HPPh_3$][Cl] (δ = 6.1 ppm in THF-d_8) together with several intractable products. Monitoring the reactions of **1** with **2a** and **2b** by ^{31}P NMR spectroscopy demonstrated that the ratio of the products **3** and **4** remained unchanged during the reactions. These observations strongly suggested that Sn−X and Sn−C_{Ar} cleaved

products **3** and **4** were formed through competitive independent pathways. Compounds **4a** and **4b** were isolated from the reactions of **1** with {*o*-(Ph_2P)C_6H_4}$_2$Sn(Ph)(X) (**5a**: X = F, **5b**: X = Cl)[18] in an excellent yield via the selective Sn−C_{Ph} bond cleavage (Scheme 5), and these molecular structures were confirmed by X-ray diffraction analysis (Figure 2).[19]

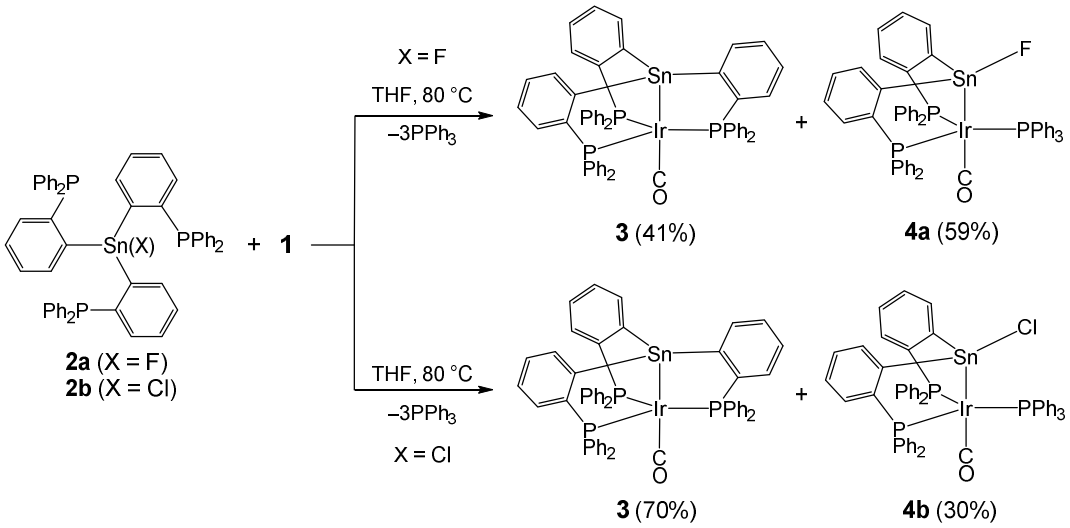

Scheme 3. Competing Sn−X and Sn−C_{Ar} σ-bond cleavages in {*o*-(Ph_2P)C_6H_4}$_3$Sn(X) (**2a**: X = F, **2b**: X = Cl) by iridium hydride **1**.

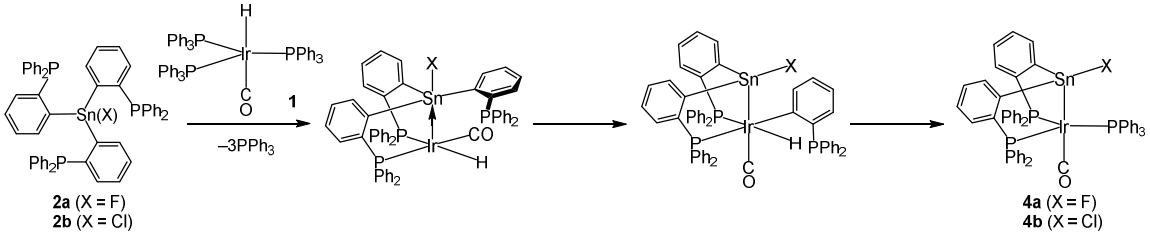

Scheme 4. Possible mechanism for the formation of **4a** and **4b**.

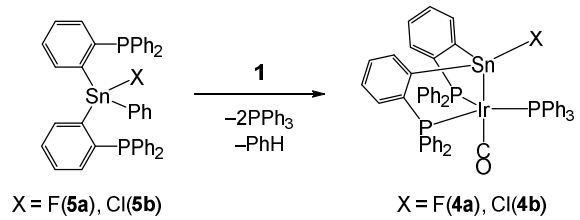

Scheme 5. Synthesis of **4a** and **4b** through exclusive Sn−C_{Ph} σ-bond cleavages in {*o*-(Ph_2P)C_6H_4}$_2$Sn(Ph)(X) (**5a**: X = F, **5b**: X = Cl) by iridium hydride **1**.

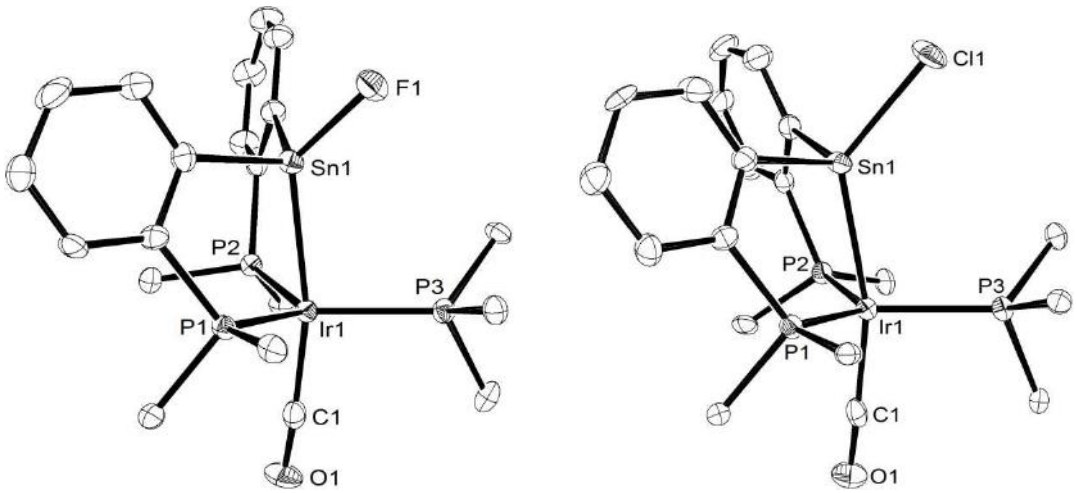

Figure 2. Molecular structures of stannyl complexes **4a** (left) and **4b** (right). Hydrogen atoms, phenyl groups (except for *ipso*-carbons), and solvent molecules are omitted for clarity. Thermal ellipsoids set at 40% probability. Selected bond distances [Å] and angles [deg]. **4a**: Ir1-Sn1: 2.5948(4), Ir1-P1: 2.3169(14), Ir1-P2: 2.3197(13), Ir1-P3: 2.3146(13), Ir1-C1: 1.875(6), Sn1-F1: 1.975(3), P1-Ir1-P2: 117.96(5), P1-Ir1-P3: 119.48(5), P2-Ir1-P3: 120.40(5), Sn1-Ir1-C1: 167.65(15). **4b**: Ir1-Sn1: 2.5794(6), Ir1-P1: 2.3248(16), Ir1-P2: 2.3291(18), Ir1-P3: 2.3331(16), Ir1-C1: 1.873(7), Sn1-Cl1: 2.4006(16), P1-Ir1-P2: 126.95(6), P1-Ir1-P3: 116.41(6), P2-Ir1-P3: 115.66(6), Sn1-Ir1-C1: 164.2(2).

Because no intermediates were detected spectroscopically in these Sn−X bond (X = F, Cl) cleavages reactions, reverse transformations, namely reactions of HX with **3**, were performed to isolate plausible intermediates. Reactions of **3** with HF·pyridine and K[HF_2] provided mainly [{*o*-(Ph_2P)C_6H_4}$_3$SnIr(H)(CO)][BF_4] (**6-BF_4**)[13] in addition to several intractable products, and the B atom in the tetrafluoroborate would stem from glass vessels. As previously reported, compound **6-BF_4** was readily synthesized from the reaction of **3** with [$HOEt_2$][BF_4],[13] and reanalysis of X-ray diffraction in this study (Figure 3a) demonstrated that one of F atoms in BF_4 weakly interacted with the stannyl moiety in the cationic part (Sn1−F1: 2.971(21) Å), which is consistent with the $^{19}F\{^1H\}$ NMR spectrum (in THF-d_8) showing two singlets at δ = −151.41 and −151.47 ppm in an intensity ratio of 1:3 (Figure S5).[20] This indicated significant Lewis acidity of the stanyl moiety in the cationic part. In contrast to the reactions with HF·pyridine and K[HF_2] affording no desired HF adduct,[21] HCl readily reacted with **3** to afford the chlorostannane complex [{*o*-(Ph_2P)C_6H_4}$_3$(Cl)Sn]Ir(H)(CO) (**7**) (Scheme 6). Compound **7** reacted with PPh_3 and NEt_3 to exclusively regenerate **3**, supporting that **7** is an intermediate for Sn−Cl bond activation. X-ray diffraction study of **7** (Figure 3b) clearly revealed the presence of Sn−Cl and Ir−H bonds, and the short Ir−Sn distance (2.8009(3) Å)[22] and the large value of the sum

of three C−Sn−C angles (358.33(17)°) imply the presence of strong dative LP(Ir)→σ*(Sn−Cl) interaction.[23,24] This was supported by significantly longer Sn−Cl bond (2.7512(7) Å) in **7** relative to that of Ph_3SnCl (2.360 Å).[25] NBO analysis of DFT computational results also supported the presence of significant LP(Ir)−σ*(Sn−Cl) CT interaction (69.4 kcal/mol)[26] (The optimized geometry (in gas phase) at B3PW91[27] (SDD(Ir, Sn), 6-311G*(P, Cl, Hydride), 6-31G*(C, O, H except Hydride)) level of theory reproduced X-ray structure well; see page S15 in Supporting Information.) CO frequency of **7** was observed at 1992 cm^{-1} (KBr pellet), which is intermediate between neutral iridium(I) **1** (1920 cm^{-1})[28] and cationic stannyl iridium(III) **6** (**6-BF_4**[13]: 2019 cm^{-1}, **6-BPh_4**: 2021 cm^{-1}) complexes. These results indicate that the coordination of Z-type stannane ligand decreases the electron density of the Ir center but its effect is less than that of stannyl cation.[29]

In contrast to the solid state, the Sn−Cl linkage would be ionized or generate a contact ion pair in solution. DFT calculations (B3PW91) in gas phase provided no stable intermediate for fluorine dissociation modeled by the elongation of the Sn−F bond, while dissociation of the Sn−Cl bond was exergonic in tetrahydrofuran solution (PCM model) (ΔG^0 = −1.3 kcal/mol; larger stabilization energies are observed in PBE, B3LYP, and M06 functionals; the details are shown on Page S16 in Supporting Information). $^{31}P\{^1H\}$ NMR

signals of **7** in THF-d_8 exhibited mutually-coupled resonances ($^2J_{PP}$ = 13.3 Hz) at δ 32.8 (d, 2P) and δ 33.8 (t, 1P) ppm (Figure S1 in Supporting Information), which are significantly different from those of cationic stannyl complex **6-BPh$_4$** with a non-coordinating tetraphenylborate anion (δ 25.8 (d, $^2J_{PP}$ = 9.4 Hz, 2P) and 27.4 (m, 1P)). These spectral data implied that the significant interaction of Lewis acidic moiety with the Cl atom exist even in solution, and strongly influence on the coordination environment around the iridium center.

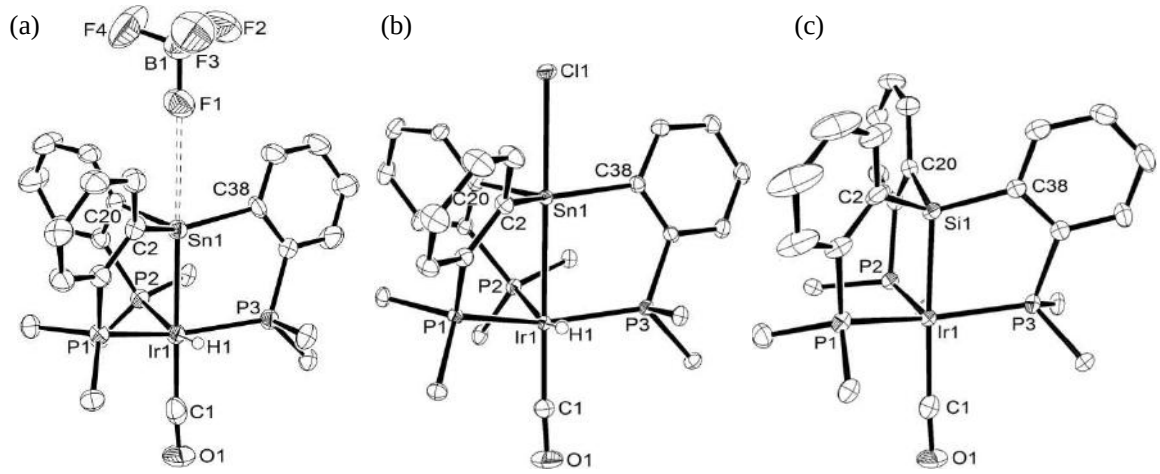

Figure 3. Molecular structures of stannyl complex **6-BF$_4$** (a),[30] stannane complex **7** (b), and silyl complex **9-Cl** (c). Hydrogen atoms (except for a hydride), phenyl groups (except for *ipso*-carbons), Cl anion, and solvent molecules are omitted for clarity. Thermal ellipsoids set at 40% probability. The hydride in **9-Cl** could not be determined by difference Fourier synthesis due to poor quality of single crystals. Selected bond distances [Å] and

angles [deg]. **6-BF$_4$**: Ir1-Sn1: 2.6290(12), Ir1-P1: 2.335(2), Ir1-P2: 2.408(3), Ir1-P3: 2.342(2), Ir1-C1: 1.931(13), Ir1-H1: 1.63(9), Sn1-F1: 2.971(21), P1-Ir1-P2: 102.99(8), P1-Ir1-P3: 145.98(9), P2-Ir1-P3: 103.54(9), P1-Ir1-C1: 97.6(3), P2-Ir1-C1: 101.5(3), P3-Ir1-C1: 97.6(3), C2-Sn1-C20: 103.3(3), C2-Sn1-C38: 133.8(3), C20-Sn1-C38: 112.1(3). **7**: Ir1-Sn1: 2.8009(3), Ir1-P1: 2.3189(7), Ir1-P2: 2.3710(7), Ir1-P3: 2.3032(7), Ir1-C1: 1.927(3), Sn1-Cl1: 2.7512(7), Ir1-H1: 1.49(4), P1-Ir1-P2: 104.14(2), P1-Ir1-P3: 143.89(2), P2-Ir1-P3: 103.21(2), P1-Ir1-C1: 98.26(9), P2-Ir1-C1: 103.14(10), P3-Ir1-C1: 98.01(9), C2-Sn1-C20: 110.20(10), C2-Sn1-C38: 132.04(10), C20-Sn1-C38: 116.09(10). **9-Cl**: Ir1-Si1: 2.368(3), Ir1-P1: 2.337(3), Ir1-P2: 2.337(3), Ir1-P3: 2.341(2), Ir1-C1: 1.962(11), P1-Ir1-P2: 105.41(9), P1-Ir1-P3: 149.51(11), P2-Ir1-P3: 100.44(9), P1-Ir1-C1: 94.3(3), P2-Ir1-C1: 102.8(4), P3-Ir1-C1: 95.5(3), C2-Si1-C20: 113.5(5), C2-Si1-C38: 113.7(5), C20-Si1-C38: 104.5(5).

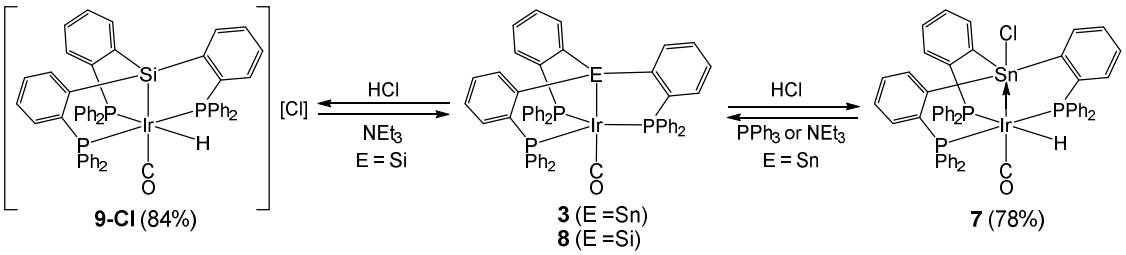

Scheme 6. Reversible HCl addition to stannyl and silyl complexes [{*o*-(Ph_2P)C_6H_4}$_3$E]Ir(CO) (**3**: E = Sn, **8**: E = Si).

Interestingly, HCl addition to the Si analogue [{*o*-(Ph_2P)C_6H_4}$_3$Si]Ir(CO) (**8**) of **3** provided the cationic silyl complex [{*o*-(Ph_2P)C_6H_4}$_3$SiIr(H)(CO)][Cl] (**9-Cl**), in which the Cl anion does not bind to silicon (Scheme 6 and Figure 3).[31] A pair of $^{31}P\{^1H\}$ resonances

in THF-d_8 at 23.2 (d, $^2J_{PP}$ = 10.6 Hz, 2P) and 24.0 (t, $^2J_{PP}$ = 10.6 Hz, 1P) of **9-Cl** is essentially the same as those of cationic silyl iridium complex [{*o*-(Ph_2P)C_6H_4}$_3$SiIr(H)(CO)][BF_4] (**9-BF$_4$**),[13] suggesting that the Cl anion does not strongly interact with the Si atom in solution either. It should be noted that the stannyl moiety in **3** exhibits larger Lewis acidity than the silyl moiety in **8** toward Cl anion, although Cl atoms generally make stronger bonds with Si than with Sn atoms. This has probably to do with the Ir−Si/Sn interactions which affect the Lewis acidity of the group 14 element, as well as the geometric constraints associated with the cage structure of the complexes.

To consider the reaction mechanism of Sn−F and Sn−Cl bond activations, we performed DFT(B3PW91) calculation using model compounds, where phenyl groups on phosphine ligands were replaced by methyl groups.[32] Considering reactions of **1** with **5a** and **5b** did not provide the products of Sn−X bond cleavage (X = F, Cl), the coordination of three phosphine arms was essential for inducing Sn−F and Sn−Cl bond cleavage. Hence we considered pathways starting from a model {(*o*-$Me_2PC_6H_4$)$_3$(Cl)Sn}Ir(H)(CO) (**B1**) for **7** and its F analogue {(*o*-$Me_2PC_6H_4$)$_3$(F)Sn}Ir(H)(CO) (**A1^{Sn}**) (Figure 4). Due to difficulty in locating pathways for Sn-X bond cleavage in gas phase, we included solvent effect using

PCM (THF solution) for optimizing all model compounds. Prior to bond cleavage, phosphine exchange between Ir(H)(CO)(PMe_3)$_3$ with (*o*-$Me_2PC_6H_4$)$_3$Sn(X) (X = F, Cl) takes place with significantly negative Gibbs energy change to afford **A1^{Sn}** and **B1**, respectively (**A1^{Sn}**: ΔG^0 = −36.8 kcal/mol in Figure 5, **B1**: ΔG^0 = −37.4 kcal/mol in Figure 6). This Gibbs energy change is much more negative than that in the reaction of Ir(H)(CO)(PMe_3)$_3$ with Si analogue (*o*-$Me_2PC_6H_4$)$_3$Si(F) (ΔG^0 = −20.0 kcal/mol) (Figure 5), which is attributed to the relatively higher stability of hypervalent structure of tin than that of silicon. The presence of significant d(Ir)→σ*(Sn−X) charge transfer (CT) interactions (X = F, Cl) was confirmed not only in **B1** but also in **A1^{Sn}**; LP(Ir)→σ*(Sn−F) and LP(Ir)→σ*(Sn−Cl) CT interactions were evaluated by NBO to be 58.7 and 101.1 kcal/mol, respectively.

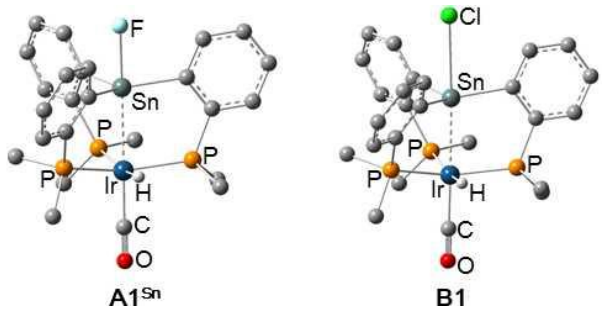

Figure 4. Optimized structures of {(*o*-$Me_2PC_6H_4$)$_3$(F)Sn}Ir(H)(CO) (**A1^{Sn}**) and {(*o*-$Me_2PC_6H_4$)$_3$(Cl)Sn}Ir(H)(CO) (**B1**) from the B3PW91 functional. Hydrogen atoms

except for hydrides are omitted for clarity.

First, we investigated an S_N2-type pathway starting from **A1^{Sn}** for Sn−F bond cleavage. However, models bearing the elongated Sn−F bond did not provide any stable intermediates, indicating that the possibility of S_N2-type pathway for Sn−F bond cleavage was ruled out. Second, σ-bond metathesis involving Ir−H and Sn−F bonds was considered (Figure 5). This reaction takes place via transition state **TS$_{A1/A2}^{Sn}$** to afford **A2^{Sn}** with a Gibbs activation energy ($\Delta G^{0‡}$) of 25.4 kcal/mol and a Gibbs reaction energy (ΔG^0) of 14.0 kcal/mol. In the Sn−F bond activation process, the geometry around the Ir atom changes from octahedron to trigonal pyramid geometry, in which three P−Ir−P angles are averaged (P−Ir−P angles[°]. **A1^{Sn}**: 151.9, 101.5, 99.5. **A2^{Sn}**: 140.5, 106.9, 106.2). Although this geometrical change alleviates the distortion around Sn, the bond activation process of Sn−F bond is uphill in Gibbs free energy, which is marked contrast with previously reported Si−F bond activation (vide infra). The subsequent elimination process of HF from **A2^{Sn}** to **A3^{Sn}** is further uphill in Gibbs energy by 1.0 kcal/mol. Probably, the subsequent reaction of HF with PPh_3 drives the Sn−F cleavage reaction forward,[33] despite the unfavorable energetic balance. Although this pathway is basically similar to Si−F bond cleavage in {*o*-$(Ph_2P)C_6H_4$}$_3$Si(F) by **1**,[10c] we

found two significant differences between Si−F bond and Sn−F bond cleavages (Figure 5); (i) The Gibbs activation energy is significantly larger in Sn−F bond cleavage than in Si−F bond cleavage and the Gibbs reaction energy is positive in Sn−F bond cleavage but negative in Si−F bond cleavage, although Si−F bond is much stronger than Sn−F bond. (ii) The intermediate $\mathbf{A4}^{\mathbf{Sn}}$ is absent (corresponding to the intermediate $\mathbf{A4}^{\mathbf{Si}}$ in the Si−F bond cleavage) prior to Sn−F bond cleavage. These differences are attributed to significantly high stability of $\mathbf{A1}^{\mathbf{Sn}}$ bearing a pentacoordinate tin center owing to the larger tendency of tin versus silicon to form hypervalent structures.[34,35] This feature would be responsible for the isolation of a plausible intermediate of stannane complex **7**, while that of the corresponding Si analogue was impracticable.

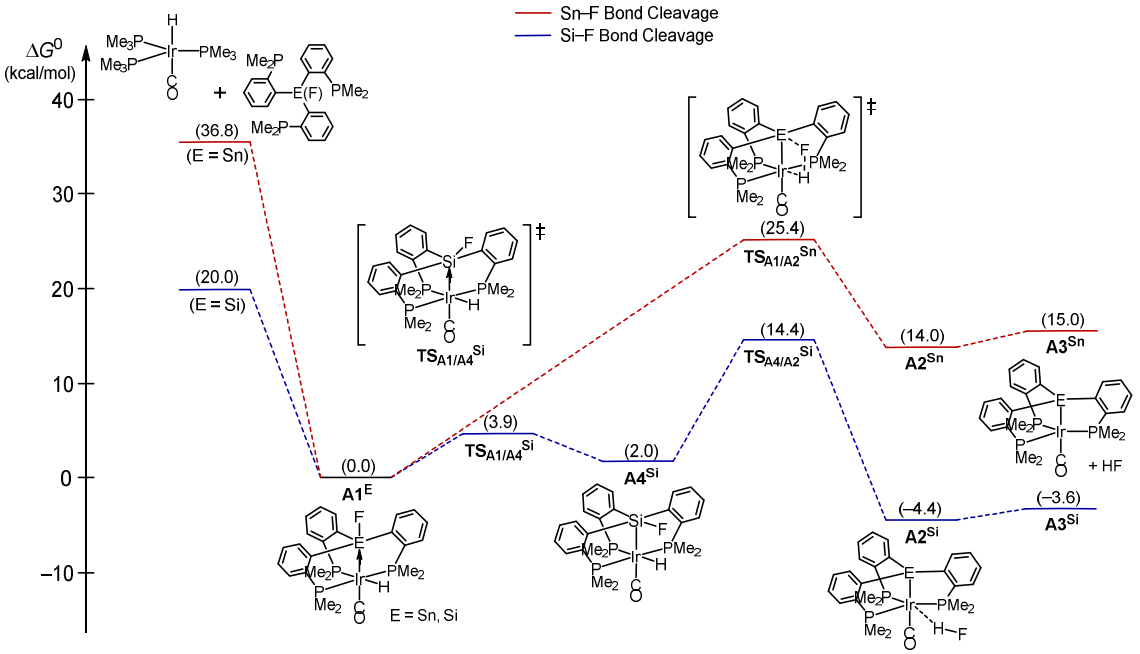

Figure 5. Comparison of energy profiles between Sn−F and Si−F bond cleavages.

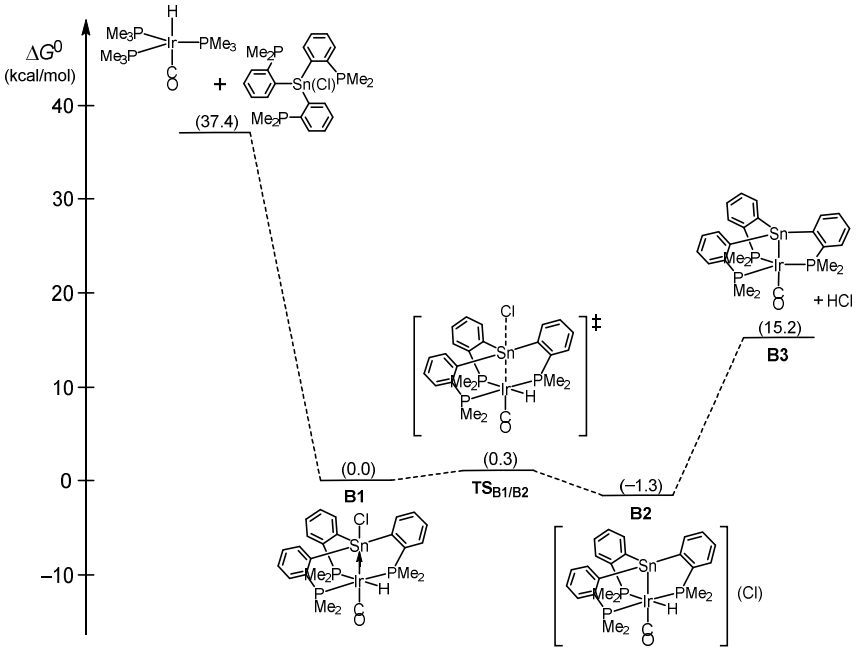

Figure 6. Energy profiles for Sn−Cl bond cleavage.

Next, the reaction of Sn−Cl bond activation starting from **B1** was investigated (Figure 6). Unlike Sn−F bond activation, no pathway involving σ-bond metathesis was found on the potential energy surface but an S_N2-type transition state $\mathbf{TS_{B1/B2}}$ was located. The Gibbs activation energy is very small ($\Delta G^{0‡}$ = 0.3 kcal/mol) and the Gibbs free energy is slightly negative (ΔG^0 = −1.3 kcal/mol). Although the subsequent HCl elimination was significantly endergonic (ΔG^0 = 16.5 kcal/mol), it is likely that PPh_3 acts as an acceptor and/or scavenger of HCl to make the reaction feasible in a similar way to that proposed for the Sn−F bond cleavage.[33] DFT computational results of Sn−Cl bond activation are basically consistent with the early study on Sn−Cl bond activation[36] by Pt complexes, in which S_N2-type pathway was proposed.[36d] The mechanistic difference between Sn−F and Sn−Cl bond activation would be attributed to the bonding natures of the Ir→Sn−X interactions, and the simultaneous formation of strong H−F bond appears to be required for the cleavage of stronger Sn−F bond than Sn−Cl bond.

CONCLUSION

In conclusion, we report here challenging Sn−F bond cleavage reaction by a late transition metal, and this is, to our knowledge, the first example of iridium-mediated Sn−F

bond cleavage with a four-coordinate stannane. Thanks to phosphine chelation, the iridium hydride **1** cleaves the Sn−F bond of fluorostannane **2a** and Sn−Cl bond of chlorostannane **2b** to afford the stannyl complex **3** and HX (H = F, Cl). Addition of HCl to **3** provided a plausible intermediate **7**, which readily regenerated **3** upon treatment with Brønsted bases. The addition and elimination of HCl induce reversible interconversion between X-type stannyl to Z-type stannane ligands. This phenomenon is reminiscent of the coordination behavior of Sb-based ligands recently reported by Gabbaï et al.,[37] but such a coordination switch was unprecedented with Sn-based ligands. DFT calculations support that the pentacoordinate species featuring a dative LP(Ir)−σ*(Sn−X) interaction (X = F, Cl) are key intermediates, and that Sn−F and Sn−Cl bond cleavages operate via two different pathways, namely σ-bond metathesis and S_N2-type reaction.[38] Sn−F bond cleavage by transition metals potentially would provide novel synthetic strategy for tin compounds, and we are working on its applications to asymmetric synthesis and multi-component coupling reaction.

General procedures. All experiments were performed under dry nitrogen atmosphere using standard Schlenk techniques. Diethylether, tetrahydrofuran, toluene, benzene-d_6, and

tetrahydrofuran-d_8 were dried over sodium and distilled under a dinitrogen atmosphere. Chloroform-*d* and dichloromethane were dried over 4Å molecular sieves. The other reagents used in this study were purchased from commercial sources and used without further purification. ^{1}H, ^{13}C{^{1}H}, ^{19}F{^{1}H}, ^{31}P{^{1}H}, and ^{119}Sn{^{1}H} NMR spectra were recorded with a JEOL JNM-AL 400 spectrometer. The ^{1}H and ^{13}C{^{1}H} NMR data were analyzed with reference to the residual peaks of the solvent, and the ^{19}F{^{1}H}, ^{31}P{^{1}H}, and ^{119}Sn{^{1}H} NMR chemical shifts were referenced to external hexafluorobenzene (−164.9 ppm), 85% H_3PO_4 (0 ppm), and tetramethylstannane (0 ppm) samples, respectively. Elemental analyses were conducted using a J-Science Lab JM-10 or FISONS Instrument EA1108 elemental analyzer. IR measurements were performed by the KBr pellet method. {*o*-(Ph_2P)C_6H_4}Li·Et_2O,[17] Ir(H)(CO)(PPh_3)$_3$ (**1**),[28] and {*o*-(Ph_2P)C_6H_4}$_3$Sn(F) (**2a**),[12] {*o*-(Ph_2P)C_6H_4}$_3$Sn(Cl) (**2b**),[17] [{*o*-(Ph_2P)C_6H_4}$_3$E]Ir(CO) (**3**: E = Sn, **8**: E = Si),[13] and [{*o*-(Ph_2P)C_6H_4}$_3$SnIr(H)(CO)][BF_4] (**6-BF_4**)[13] were prepared as described in the literature.

Preparation of {(*o*-Ph_2P)C_6H_4}$_2$Sn(Ph)(Cl) (5b) A Schlenk tube was charged with {*o*-(Ph_2P)C_6H_4}Li·Et_2O (481 mg, 1.40 mmol), toluene (12 mL), and the solution was cooled to −78 °C. $PhSnCl_3$ (0.63 mmol), 1 M solution in toluene, was added slowly to the prepared reaction solution, and the mixture was allowed to room temperature. The reaction

mixture was stirred at 100 °C for 14 h. The solution was filtered and the volatile materials were removed under vacuum to afford a white solid. The residue was washed with a 1:5 mixture of ether and *n*-hexane (6 mL×3), and dried under vacuum to afford **5b** (344 mg, 0.458 mmol) in 73 % yield as a white powder. ^{1}H NMR (400 MHz, $CDCl_3$): δ 6.86-7.43 (m, 29H), 7.84 (d, J = 7.4 Hz, 2H), 7.96 (d, J = 7.1 Hz, 2H). ^{13}C{^{1}H} NMR (100 MHz, $CDCl_3$): δ 128.4 (m), 128.5 (m), 128.8 (s), 129.2 (s), 130.2 (d, $J_{P\text{-}C}$ = 20.7 Hz), 133.0 (m), 133.5 (m), 134.4 (s, $J_{C\text{-}119Sn}$ = 62.8 Hz), 136.0 (m), 136.7 (t, $J_{P\text{-}C}$ = 18.1 Hz), 136.8 (m), 142.3 (t, $J_{P\text{-}C}$ = 6.6 Hz), 143.6 (d, $J_{P\text{-}C}$ = 1.7 Hz, $J_{C\text{-}119Sn}$ = 69.4 Hz), 155.1 (dd, $J_{P\text{-}C}$ = 76.8, 6.6 Hz). ^{31}P{^{1}H} NMR (162 MHz, $CDCl_3$): δ 2.0 (s, $J_{P\text{-}119Sn}$ = 13.9 Hz). ^{119}Sn{^{1}H} NMR (187 MHz, $CDCl_3$): δ −100.1 (t, $J_{P\text{-}119Sn}$ = 13.9 Hz). Anal. Calcd for $C_{42}H_{33}ClP_2Sn$: C, 66.92; H, 4.41. Found: C, 66.71; H, 4.45.

Preparation of {(*o*-Ph$_2$P)C$_6$H$_4$}$_2$Sn(Ph)(F) (5a) A Schlenk tube was charged with **5b** (336 mg, 0.446 mmol), CsF (351 mg, 2.31 mmol), and toluene (25 mL). After stirring at 50 °C for 76 h, the volatile materials were removed under vacuum to afford a white solid. The residue was washed with methanol (4 mL × 3) and a 1:3 mixture of ether and *n*-hexane (4 mL × 3), and dried under vacuum to afford **5a** (215 mg, 0.292 mmol) in 66% yield as a white powder. ^{1}H NMR (400 MHz, $CDCl_3$): δ 6.92-7.30 (m, 25H), 7.35-7.45 (m, 4H), 7.79

(d, J = 6.4 Hz, 2H), 7.90 (d, J = 7.2 Hz, 2H). $^{13}C\{^{1}H\}$ NMR (100 MHz, $CDCl_3$): δ 128.4 (m), 128.6 (s), 128.8 (s), 129.1 (s), 130.2 (d, $J_{P\text{-}C}$ = 10.5 Hz), 133.0 (t, $J_{P\text{-}C}$ = 8.1 Hz), 133.5 (t, $J_{P\text{-}C}$ = 9.1 Hz), 134.1 (s, $J_{C\text{-}119Sn}$ = 63.0 Hz), 135.9 (m), 136.5 (t, $J_{P\text{-}C}$ = 18.7 Hz), 136.9 (m), 142.5 (m), 143.8 (s, $J_{C\text{-}119Sn}$ = 36.3 Hz), 155.9 (dd, $J_{P\text{-}C}$ = 86.8, 15.2 Hz). $^{19}F\{^{1}H\}$ NMR (376 MHz, $CDCl_3$): δ −214.1 (t, $J_{P\text{-}F}$ = 39.1 Hz, $J_{119Sn\text{-}F}$ = 2359.0 Hz). $^{31}P\{^{1}H\}$ NMR (162 MHz, $CDCl_3$): δ 4.1 (d, $J_{P\text{-}F}$ = 39.1 Hz). $^{119}Sn\{^{1}H\}$ NMR (187 MHz, $CDCl_3$): δ −143.3 (d, $J_{119Sn\text{-}F}$ = 2359.0 Hz). Anal. Calcd for $C_{42}H_{33}FP_2Sn$: C, 68.41; H, 4.51. Found: C, 68.21; H, 4.48.

Preparation of [{(*o*-Ph_2P)C_6H_4}$_2$Sn(F)]Ir(CO)(PPh_3) (4a) A Schlenk tube was charged with Ir(H)(CO)(PPh_3)$_3$ (**1**) (129.0 mg, 0.128 mmol), **5a** (98.7 mg, 0.134 mmol), and toluene (10 mL). After stirring at 80 °C for 18 h, the volatile materials were removed under vacuum to afford a yellow residue. The residue was washed with *n*-hexane (4 mL × 3), and dried under vacuum to afford **4a** (135.0 mg, 0.118 mmol) in 92% yield as yellow solid. ^{1}H NMR (400 MHz, $CDCl_3$): δ 6.67-6.73 (m, 4H), 6.85-7.02 (m, 20H), 7.05-7.19 (m, 9H), 7.23-7.30 (m, 4H), 7.47-7.53 (m, 4H), 8.29 (d, J = 6.8 Hz, 2H). $^{13}C\{^{1}H\}$ NMR (100 MHz, $CDCl_3$): δ 127.6 (d, $J_{P\text{-}C}$ = 10.5 Hz), 127.7 (t, $J_{P\text{-}C}$ = 4.8 Hz), 128.4 (m), 128.7 (m), 130.2 (s), 131.6 (t, $J_{P\text{-}C}$ = 3.3 Hz), 132.2 (m), 132.8 (d, $J_{P\text{-}C}$ = 13.4 Hz), 133.2 (t, $J_{P\text{-}C}$ = 6.7 Hz), 135.0 (m),

138.5 (t, $J_{P\text{-}C}$ = 24.8 Hz), 139.1 (d, $J_{P\text{-}C}$ = 41.1 Hz), 140.6 (m), 141.8 (m), 161.5 (m), 188.9 (m, CO). $^{19}F\{^{1}H\}$ NMR (376 MHz, $CDCl_3$): δ −212.0 (dt, $J_{P\text{-}F}$ = 11.7 Hz, 9.8 Hz, $^{1}J_{117Sn\text{-}F}$ = 2474.3 Hz, $^{1}J_{119Sn\text{-}F}$ = 2598.1 Hz). $^{31}P\{^{1}H\}$ NMR (162 MHz, $CDCl_3$): δ 11.2 (td, $^{2}J_{P\text{-}P}$ = 88.8 Hz, $J_{P\text{-}F}$ = 11.7 Hz, PPh_3), 46.6 (dd, $^{2}J_{P\text{-}P}$ = 88.8 Hz, $J_{P\text{-}F}$ = 9.8 Hz, PPh_2). Anal. Calcd for $C_{55}H_{43}OFIrP_3Sn$: C, 57.81; H, 3.79. Found: C, 57.82; H, 3.94. IR (KBr, cm^{-1}) *ν* (CO): 1964 cm^{-1}. $^{119}Sn\{^{1}H\}$ NMR data of **4a** is not available due to the low solubility in organic solvents.

Preparation of [{(*o*-Ph_2P)C_6H_4}$_2$Sn(Cl)]Ir(CO)(PPh_3) (4b) A Schlenk tube was charged with Ir(H)(CO)(PPh_3)$_3$ (**1**) (68.4 mg, 0.0677 mmol), **5b** (93.3 mg, 0.0711 mmol), and toluene (5 mL). After stirring at 80 °C for 18 h, the volatile materials were removed under vacuum to afford a yellow residue. The residue was washed with *n*-hexane (4 mL × 3), and dried under vacuum to afford **4b** (73.4 mg, 0.0633 mmol) in 94% yield as yellow solid. ^{1}H NMR (400 MHz, $CDCl_3$): δ 6.66-6.73 (m, 4H), 6.96-7.02 (m, 20H), 7.05-7.12 (m, 9H), 7.24-7.30 (m, 4H), 7.43-7.53 (m, 4H), 8.31 (d, *J* = 6.8 Hz, 2H). $^{13}C\{^{1}H\}$ NMR (100 MHz, $CDCl_3$): δ 127.6 (d, $J_{P\text{-}C}$ = 10.0 Hz), 127.8 (t, $J_{P\text{-}C}$ = 4.8 Hz), 128.5 (m), 130.5 (s), 131.6 (t, $J_{P\text{-}C}$ = 6.0 Hz), 132.1 (s), 133.0 (d, $J_{P\text{-}C}$ = 12.9 Hz), 133.2 (t, $J_{P\text{-}C}$ = 7.2 Hz), 135.6 (t, $J_{P\text{-}C}$ = 11.7 Hz), 138.3 (t, $J_{P\text{-}C}$ = 25.3 Hz), 138.4 (d, $J_{P\text{-}C}$ = 41.5 Hz), 140.1 (m), 141.7 (m),

161.0 (m), 188.3 (m, CO). $^{31}P\{^{1}H\}$ NMR (162 MHz, $CDCl_3$): δ 11.8 (t, $^{2}J_{P\text{-}P}$ = 89.2 Hz, PPh_3), 46.0 (d, $^{2}J_{P\text{-}P}$ = 89.2 Hz, PPh_2). Anal. Calcd for $C_{55}H_{43}OClIrP_3Sn$: C, 56.99; H, 3.74. Found: C, 56.99; H, 3.99. IR (KBr, cm^{-1}) *v* (CO): 1969 cm^{-1}. $^{119}Sn\{^{1}H\}$ NMR data of **4b** is not available due to the low solubility in organic solvents.

Preparation of [{(*o*-Ph_2P)C_6H_4}$_3$Sn(Cl)]IrH(CO) (7) A Schlenk tube was charged with {(*o*-$Ph_2PC_6H_4$)$_3$Sn}Ir(CO) (53.7 mg, 0.0478 mmol) and tetrahydrofuran (5 mL). After addition of HCl (1M diethylether solution, 0.15 ml), the reaction mixture was allowed to stir at ambient temperature for 15 h. After the volatile materials were removed under vacuum, the white residue was washed with Et_2O (5 mL). Slow diffusion of n-hexane into dichloromethane solution of the residue afforded **7** (43.2 mg, 0.0377 mmol) in 78% yield as colorless crystals. ^{1}H NMR (400 MHz, $CDCl_3$): δ −12.28 (td, $J_{P\text{-}H}$= 97.2Hz, $J_{P\text{-}H}$ = 18.8Hz, 1H, Ir-H), 6.47 (t, *J* = 7.4 Hz, 1H), 6.73-6.80 (m, 3H, Ar), 6.83-6.92 (m, 17H, Ar), 7.07-7.13 (m, 6H, Ar), 7.21-7.33 (m, 10H, Ar), 7.52 (t, *J* = 7.2Hz, 2H, Ar), 9.12 (d, *J* = 7.2Hz, 1H, Ar), 9.40 (d, *J* = 7.6Hz, 2H, Ar). $^{13}C\{^{1}H\}$ NMR (100 MHz, $CDCl_3$): δ 127.5 (m), 127.8 (d, $J_{P\text{-}C}$ = 9.9 Hz), 128.2 (m), 128.4 (m), 129.2-130.9 (6 overlapping), 132.6 (m), 132.7 (m), 133.5 (d, $J_{P\text{-}C}$ = 10.0 Hz), 138.7 (d, $J_{P\text{-}C}$ = 19.3 Hz), 139.0 (d, $J_{P\text{-}C}$ = 6.9Hz), 139.0 (d, $J_{P\text{-}C}$ = 6.9 Hz), 139.2 (m), 139.6 (m), 141.2 (t, $J_{P\text{-}C}$ = 36.2 Hz), 154.1 (m), 154.8 (t,

$J_{P\text{-}C}$ = 20.5 Hz), 177.1 (td, $J_{P\text{-}C}$ = 3.6Hz, $J_{P\text{-}C}$ = 1.5Hz, CO). $^{31}P\{^{1}H\}$ NMR (162 MHz, THF-d_8): δ 32.8 (d, $^{2}J_{P\text{-}P}$ = 13.3 Hz, PPh_2), 33.8 (t, $^{2}J_{P\text{-}P}$ = 13.3 Hz, PPh_2). Anal. Calcd for $C_{55}H_{43}OClIrP_3Sn$: C, 56.99; H, 3.74. Found: C, 56.79; H, 3.70. IR (KBr, cm^{-1}) ν (CO): 1992 cm^{-1}. $^{119}Sn\{^{1}H\}$ NMR data of **7** is not available due to the low solubility in organic solvents.

Preparation of [{(*o*-$Ph_2PC_6H_4)_3Si$}IrH(CO)][Cl] (9-Cl) A Schlenk tube was charged with {(*o*-$Ph_2PC_6H_4)_3Si$}Ir(CO) (34.0 mg, 0.0329 mmol) and tetrahydrofuran (2 mL). After addition of HCl (1M diethylether solution, 0.10 ml), the reaction mixture was allowed to stir at ambient temperature for 15 h. After the volatile materials were removed under vacuum, the white residue was washed with Et_2O (3 mL). Slow diffusion of *n*-hexane into dichloromethane solution of the residue afforded **9-Cl** (29.2 mg, 0.0278 mmol) in 84% yield as colorless crystals. ^{1}H, $^{31}P\{^{1}H\}$ NMR and IR spectra are essentially the same as those of [{(*o*-$Ph_2PC_6H_4)_3Si$}IrH(CO)][BF_4] (**9-BF_4**).[13]

Reactions of 7 with Brønsted Bases. (i) Reaction of 7 with NEt_3. An NMR tube was charged with **7** (5.9 mg, 0.0050 mmol) and tetrahydrofuran (0.50 mL), and a capillary filled with a toluene solution of trimesitylphosphine was placed in the NMR tube as an internal standard. Addition of NEt_3 (2.2 μL, 0.016 mmol) to the mixture immediately resulted in the

quantitative formation of **3**. **(ii) Reaction of 7 with PPh_3.** An NMR tube was charged with **7** (5.9 mg, 0.0050 mmol), PPh_3 (4.1 mg, 0.016 mmol) and tetrahydrofuran (0.50 mL), and a capillary filled with a toluene solution of trimesitylphosphine was placed in the NMR tube as an internal standard. The reaction was performed at 80 °C for 24 hours to afford **3** quantitatively.

Anion (BF_4/BPh_4) Exchange of 6-BF_4. A Schlenk tube was charged with **6-BF_4** (20.1 mg, 0.0166 mmol), $NaBPh_4$ (56.5 mg, 0.165 mmol), and methanol (2 mL). After the reaction mixture was allowed to stir at ambient temperature for 24 h, the volatile materials were removed under vacuum. The white residue was washed with methanol (2 mL x 3) to afford **6-BPh_4** (19.8 mg, 0.0137 mmol) in 83% yield as white solid. **6-BPh_4**: ^{1}H NMR (400 MHz, THF-d_8): δ −12.44 (td, $J_{P\text{-}H}$= 98.9Hz, $J_{P\text{-}H}$ = 18.9Hz, 1H, Ir-H), 6.65-7.43 (m, 57H, Ar), 7.66 (t, J = 7.3Hz, 2H, Ar), 8.31 (d, J = 7.9Hz, 1H, Ar), 8.59 (d, J = 7.3Hz, 2H, Ar). ^{31}P{^{1}H} NMR (162 MHz, THF-d_8): δ 25.9 (d, $^2J_{PP}$ = 9.4 Hz, 2P), 27.2 (m, 1P). Anal. Calcd for $C_{79}H_{63}BIrOP_3Sn$: C, 65.76; H, 4.40. Found: C, 65.99; H, 4.53. IR (KBr, cm^{-1}) ν (CO): 2021 cm^{-1}.

Determination of NMR yield. (a) Reaction of 1 with 2a. An NMR tube was charged with **1** (5.0 mg, 0.0050 mmol), **2a** (4.6 mg, 0.0050 mmol), and tetrahydrofuran (0.50 mL),

and a capillary filled with a toluene solution of trimesitylphosphine was placed in the NMR tube as an internal standard. The reaction at 80 °C was monitored by ^{31}P NMR spectroscopy. After 30 hours, **3** and **4a** were formed in 41% and 59% NMR yield, respectively. **(b) Reaction of 1 with 2b.** An NMR tube was charged with **1** (5.0 mg, 0.0050 mmol), **2b** (4.6 mg, 0.0049 mmol), and tetrahydrofuran (0.50 mL), and a capillary filled with a toluene solution of trimesitylphosphine was placed in the NMR tube as an internal standard. The reaction at 80 °C was monitored by ^{31}P NMR spectroscopy. After 32 hours, **3** and **4b** were formed in 70% and 30% NMR yield, respectively.

Structure Determination by X-ray Diffraction. Suitable single crystals of **4a**, **4b**, **7**, **9-Cl**, and **9-BF$_4$** were obtained from the slow diffusion of *n*-hexane into a dichloromethane solution (**4a**, **4b**, and **7**), a chloroform solution (**9-Cl**), a tetrahydrofuran solution (**9-BF$_4$**), and a tetrahydrofuran/dioxane mixed solution (**6-BF$_4$**). Diffraction intensity data were collected with a Rigaku/MSC Mercury CCD diffractometer at 200 K (**4a** and **4b**), a Rigaku/Saturn724 CCD diffractometer at 200 K (**6-BF$_4$** and **9-BF$_4$**), and a Rigaku/R-AXIS RAPID IP diffractometer at 173 K (**7** and **9-Cl**), and a semiempirical multi-scan absorption[39] correction was performed. The space groups were chosen based on the systematic absences in the diffraction data. The structures were solved using SIR97[40] by

subsequent difference Fourier synthesis, and refined by full matrix least-squares procedures on F^2. All non-hydrogen atoms were refined with anisotropic displacement coefficients. The hydrogen atoms except for hydrides were treated as idealized contributions and refined in rigid group model. The hydride ligands in **7** and **9-BF$_4$** was determined by difference Fourier synthesis and refined isotropically. All software and sources of scattering factors are contained in the SHELXL97 program package.[41] CCDC 1520115 (**4a**), 1520116 (**4b**), CCDC 1533991 (**9-BF$_4$**), 1533992 (**6-BF$_4$**), 1533993 (**7**), and 1533994 (**9-Cl**) contain supplementary crystallographic data for this paper. These data can be obtained free of charge from the Cambridge Crystallographic Data Centre via www.ccdc.cam.ac.uk/data_request/cif.

Density Functional Theory (DFT) Calculation. The Gaussian09 program was employed for all calculations here.[42] All of the geometry optimizations were performed by the density functional theory (DFT) with the B3PW91 functional in THF solution, where the polarizable continuum model (PCM)[43] was used to calculate solvation effect. The effective core potentials (ECPs) of the Stuttgart-Dresden-Bonn group were employed for the core electrons of iridium and tin and the corresponding basis sets[44] were used for the valence electrons. Usual 6-311G(d,p) basis sets[45] were used for all other atoms. The

vibrational frequencies were calculated to identify the structure in the equilibrium state, i.e., the structure that was true minima or transition states. Here, the Gibbs activation energy ($\Delta G^{\circ\ddagger}$) is defined as a difference in the Gibbs energy at 298.15 K between a transition state and an intermediate, when the intermediate exists before the transition state and it is more stable than the reactant. Otherwise, $\Delta G^{\circ\ddagger}$ is defined as the Gibbs energy difference between the transition state and the reactant. The Gibbs reaction energy (ΔG°) is defined as the difference in Gibbs energy between the product and the reactant. In the calculation, we employed model compounds where the phenyl groups of the phosphine were replaced by methyl groups to save the CPU time.

ASSOCIATED CONTENT

Supporting Information

Crystallographic data, Computational details. Crystallographic data are also available in CIF format.

The Supporting Information is available free of charge on the ACS Publications website.

AUTHOR INFORMATION

Corresponding Author

*E-mail: h.kameo@c.s.osakafu-u.ac.jp

Notes

The authors declare no competing financial interest.

ACKNOWLEDGMENT

This research was supported by a Grant-in-Aid for Scientific Research (C) (No. 15K05458 and 15K05459) from Japan Society for the promotion of Science (JSPS) and by Grant-in-Aid for that Scientific Research on Innovative Areas “Stimuli-responsive Chemical Species for the Creation of Functional Molecules” (No. 15H00940, 15H00957, and 15H00958) from the Ministry of Education, Science, Sports, and Culture of Japan (MEXT).

REFERENCES

(1) (a) Crabtree, R. H. *Organometallic Chemistry of the Transition Metals*, *6th ed*., John Wiley & Sons, Inc., New Jersey, 2014; (b) Hartwig, J. F. *Organotransition Metal Chemistry*

from Bonding to Catalysis, University Science Books, Sausalito, 2010.

(2) Apeloig, Y. in *The Chemistry of Organic Silicon Compounds,* Vol. 1 (Eds.: Patai, S.; Rappoport, Z.), John Wiley & Sons, Inc., 1989, Chapter 2.

(3) Bond dissociation energies: $D_{Si–F}$ = 540 kJ/mol, $D_{Ge–F}$ = 485 kJ/mol, $D_{Sn–F}$ = 467 kJ/mol, $D_{Si–Cl}$ = 456 kJ/mol, $D_{Ge–Cl}$ = 432 kJ/mol, $D_{Sn–Cl}$ = 406 kJ/mol: Lange's Handbook of Chemistry, 13th ed. (Eds.: N. A. Lange, J. A. Dean), McGraw-Hill, New York, 1985, pp. 3–131.

(4) (a) Sakaki, S.; Ieki, M. *J. Am. Chem. Soc.* **1993**, *115*, 2373-2381. (b) Kameo, H.; Sakaki, S. *Chem. Eur. J.* **2015**, *21*, 13588-13597.

(5) (a) Doherty, N.M.; Hoffman, N.W. *Chem. Rev.*, **1991**, *91*, 553-573; (b) Murphy, E.F.; Murugavel, R.; Roesky, H.W. *Chem. Rev.*, **1997**, *97*, 3425-3468.

(6) (a) Herzog, A.; Liu, F.-Q.; Roesky, H. W.; Demsar, A.; Keller, K.; Noltemeyer, M.; Pauer, F. *Organometallics* **1994**, *13*, 1251-1256. (b) Liu, F.-Q.; Usón, I.; Roesky, H. W. *J. Chem. Soc., Dalton Trans*, **1995**, 2453-2458. (c) Köhler, K.; Herzog, A.; Steiner, A.; Roesky, H. W. *Angew. Chem. Int. Ed. Engl.* **1996**, *35*, 295-297. (d) Murphy, E. F.; Lübben, T.;

Herzog, A.; Roesky, H. W.; Demsar, A.; Noltemeyer, M.; Schmidt, H.-G. *Inorg. Chem.* **1996**, *35*, 23-29. (e) Murphy, E. F.; Yu, P.; Dietrich, S.; Roesky, H. W.; Parisini, E.; Noltemeyer, M. *J. Chem. Soc., Dalton Trans.* **1996**, 1983-1987. (f) Liu, F.-Q.; Herzog, A.; Roesky, H. W.; Usón, I. *Inorg. Chem.* **1996**, *35*, 741-744. (g) Yu, P.; Murphy, E. F.; Roesky, H. W.; Lubini, P.; Schmidt, H.-G.; Noltemeyer, M. *Organometallics* **1997**, *16*, 313-316. (h) Pevec, A.; Demsar, A.; Gramlich, V.; Petricek, S.; Roesky, H. W. *J. Chem. Soc., Dalton Trans.* **1997**, 2215-2216. (i) Roesky, H. W. *Inorg. Chem.* **1999**, *38*, 5934-5943.

(7) Parkin et al. reported the synthesis of zinc fluoride via Sn−F bond cleavage of Me_3SnF; see Sattler, W.; Ruccolo, S.; Parkin, G. *J. Am. Chem. Soc.* **2013**, *135*, 18714-18717.

(8) DFT calculations were carried out at the B3PW91 (SDD for Ir, Sn and 6-311G* for other atoms) level of theory.

(9) Dugan, T. R.; Goldberg, J. M.; Brennessel, W. W.; Holland, P. L. *Organometallics* **2012**, *31*, 1349-1360.

(10) (a) Kameo, H.; Ishii, S.; Nakazawa, H. *Dalton Trans.* **2012**, *41*, 11386-11392. (b)

Kameo, H.; Ishii, S.; Nakazawa, H. *Dalton Trans.* **2013**, *42*, 4663-4669. (c) Kameo, H.; Kawamoto, T.; Sakaki, S.; Bourissou, D.; Nakazawa, H. *Chem. Eur. J.* **2016**, *22*, 2370-2375. (d) Kameo, H.; Ikeda, K.; Bourissou, D.; Sakaki, S.; Takemoto, S.; Nakazawa, H.; Matsuzaka, H. *Organometallics* **2016**, *35,* 713-719. (e) Kameo, H.; Ikeda, K.; Sakaki, S.; Nakazawa, H.; Takemoto, S.; Matsuzaka, H. *Dalton Trans.* **2016**, *45*, 7570-7580. (f) Kameo, H.; Nakazawa, H. *Chem. Rec.* **2017**, *17*, 268-286.

(11) Selected references for ligand classification of transition metal complexes; see (a) Green, M. L. H. *J. Organomtet. Chem.* **1995**, *500*, 127-148. (b) Hill, A. F. *Organometallics* **2006**, *25*, 4741-4743. (c) Parkin, G. *Organometallics* **2006**, *25*, 4744-4747. (d) Kuzu, I.; Krummenacher, I.; Meyer, J.; Armbruster, F.; Breher, F. *Dalton Trans.* **2008**, 5836-5865. (e) Braunschweig, H.; Dewhurst, R. D.; Schneider, A. *Chem. Rev.* **2010**, *110*, 3924-3957. (f) Owen, G. R. *Chem. Soc. Rev.* **2012**, *41*, 3535-3546. (g) Kameo, H.; Nakazawa, H. *Chem. Asian J.* **2013**, *8*, 1720-1734.

(12) Kameo, H.; Kawamoto, T.; Sakaki, S.; Nakazawa, H. *Organometallics* **2014**, *33*, 5960-5963.

(13) Kameo, H.; Ishii, S.; Nakazawa. H. *Dalton Trans.* **2012**, *41*, 8290-8296.

(14) The ratio of **3**:**4a**/**b** would be determined at the coordination step of the third phosphine arm; see page S21 in Supporting Information.

(15) Cabon, Y.; Reboule, I.; Gebbink, R. J. M. K.; Deelman, B.-J. *Organometallics*, **2010**, *29*, 5904-5911 and references for transition-metal-mediated Sn-C bond cleavage therein.

(16) Takaya, J.; Nakamura, S.; Iwasawa, N. *Chem. Lett.*, **2012**, *41*, 967-969.

(17) Kameo, H.; Ishii, S.; Nakazawa, H. *Organometallics* **2012**, *31*, 2212-2218.

(18) *i*-Pr analogues {*o*-(*i*-Pr_2P)C_6H_4}$_2$Sn(Ph)(F) and {*o*-(*i*-Pr_2P)C_6H_4}$_2$Sn(Ph)(Cl) of **2a** and **2b** were reported by Bourissou and Gabbaï, and the intramolecular P→Sn interactions in these compounds were studied. See (a) Gualco, P.; Lin, T.-P.; Sircoglou, M.; Mercy, M.; Ladeira, S.; Bouhadir, G.; Pérez, L. M.; Amgoune, A.; Maron, L.; Gabbaï, F. P.; Bourissou, D. *Angew. Chem. Int. Ed.* **2009**, *48*, 9892-9895. (b) Lin, T.-P.; Gualco, P.; Ladeira, S.; Amgoune, A.; Bourissou, D.; Gabbaï, F. P. *C. R. Chim.* **2010**, *13*, 1168.

(19) $^{31}P\{^1H\}$ NMR spectrum of **4a** and **4b** exhibited mutually-coupled resonances (**4a**: 11.2 (dt, $J_{P\text{-}F}$ = 11.7 Hz, $^2J_{P\text{-}P}$ = 88.8 Hz) and 46.6 (dd, $J_{P\text{-}F}$ = 9.8 Hz, $^2J_{P\text{-}P}$ = 88.8 Hz), **4b**: 11.8 (t, $^2J_{P\text{-}P}$ = 89.2 Hz) and 46.0 (d, $^2J_{P\text{-}P}$ = 89.2 Hz)), and $^{19}F\{^1H\}$ NMR signal of **4a** was

observed as a doublet of triplet ($J_{P\text{-}F}$ = 11.7, 9.8 Hz) with a satellite due to ^{119}Sn and ^{117}Sn ($^{1}J_{119Sn\text{-}F}$ = 2598 Hz, $^{1}J_{117Sn\text{-}F}$ = 2474 Hz) at −212.0 ppm. These spectral data are consistent with C_{2v} symmetrical structures observed for the solid states.

(20) Despite of the presence of $F_3B{-}F{\rightarrow}Sn$ interaction, $^{31}P\{^{1}H\}$ NMR spectrum (in THF-d_8) of **6-BF$_4$** (δ 25.8 (d, $^{2}J_{PP}$ = 9.4 Hz, 2P) and 27.4 (m, 1P)) is only slightly shifted in comparison with **6-BPh$_4$** (δ 25.9 (d, $^{2}J_{PP}$ = 9.4 Hz, 2P) and 27.2 (m, 1P)) with a non-coordinating tetraphenylborate anion (see page S2 in Supporting Information), presumably indicating that the $F_3B{-}F{\rightarrow}Sn$ interaction does not strongly influence coordination environment around the iridium center.

(21) Although salt metathesis reactions of [{*o*-(Ph_2P)C_6H_4}$_3$SnIr(H)(CO)][BF_4] (**7-BF$_4$**) with KF and CsF were also investigated to synthesize fluorostannane complex [{*o*-(Ph_2P)C_6H_4}$_3$(F)Sn]Ir(H)(CO), neutral complex **3** was mainly formed. Then, a broad signal was observed around δ = 16 ppm[46] ($w_{1/2}$ = 83.6 Hz, in DMSO-d_6), suggesting the formation of $[HF_2]^{-}$. These results imply that the isolation of [{*o*-(Ph_2P)C_6H_4}$_3$(F)Sn]Ir(H)(CO) is difficult due to readily elimination of HF.

(22) Ir−Sn distance (2.8009(3) Å) is almost equal to the sum of covalent atomic radii

(2.80 Å). Cordero, B.; Gómez, V.; Platero-Prats, A. E.; Revés, M.; Echeverría, J.; Cremades, E.; Barragán, F.; Alvarez, S. *Dalton Trans.* **2008**, *37*, 2832.

(23) We reported that iridium hydride **1** also formed a dative metal→Z interaction (Z = Z-type (σ-electron acceptor) ligand) in the reactions with di- and triphosphine borane; see (a) Kameo, H.; Nakazawa, H. *Organometallics* **2012**, *31*, 7476-7484. (b) Kameo, H.; Hashimoto, Y.; Nakazawa, H. *Organometallics* **2012**, *31*, 4251-4258.

(24) Examples bearing a dative M→E interaction (E = heavier group 14 element compounds) have been studied by several groups; see (a) Grobe, J.; Krummen, N.; Wehmschulte, R. W.; Krebs, B.; Laege, M. *Z. Anorg. Allg. Chem.* **1994**, *620*, 1645-1658. (b) Grobe, J.; Wehmschulte, R.; Krebs, B.; Läge, M. *Z. Anorg. Allg. Chem.* **1995**, *621*, 583-596. (c) Grobe, J.; Lütke-Brochtrup, K.; Krebs, B.; Läge, M.; Niemeyer, H. -H., Würthwein, E. -U. *Z. Naturforsch.* **2007**, *62b*, 55-65. (d) Wagler, J.; Hill, A. F.; Heine, T. *Eur. J. Inorg. Chem.* **2008**, 4225-4229. (e) Wagler, J.; Bredler, E. *Angew. Chem. Int. Ed.* **2010**, *49*, 624-627. (f) Cabon, Y.; Kleijn, H.; Siegler, M. A.; Spek, A. L.; Gebbink, R. J. M. K.; Deelman, B.-J. *Dalton Trans.* **2010**, *39*, 2423–2427. (g) Gualco, P.; Mercy, M.; Ladeira, S.; Coppel, Y.; Maron, L.; Amgoune, A.; Bourissou, D. *Chem. Eur. J.* **2010**, *16*,

10808-10817. (h) Truflandier, L. A.; Brendler, E.; Wagler, J.; Autschbach, J. *Angew. Chem. Int. Ed.* **2011**, *50*, 255-259. (i) Derrah, E. J.; Sircoglou, M. M.; Mercy, M.; Ladeira, S.; Bouhadir, G.; Miqueu, K.; Maron, L.; Bourissou, D. *Organometallics* **2011**, *30*, 657-660. (i) Brendler, E.; Wächtler, E.; Heine, T.; Zhechkov, L.; Langer, T.; Pöttgen, R.; Hill, A. F.; Wagler, J. *Angew. Chem. Int. Ed.* **2011**, *50*, 4696–4700. (j) Sakaki, S.; Kawai, D.; Tsukamoto, S. *Collect. Czech. Chem. Commun.* **2011**, *76*, 619–629. (k) Martincová, J.; Dostál, L.; Herres-Pawlis, S.; Růžička, A.; Jambor, R. *Chem. Eur. J.* **2011**, *17*, 7423-7427. (l) Kano, N.; Yoshinari, N.; Shibata, Y.; Miyachi, M.; Kawashima, T.; Enomoto, M.; Okazawa, A.; Kojima, N.; Guo, J. -D.; Nagase, S. *Organometallics* **2012**, *31*, 8059-8062. (m) Autschbach, J.; Sutter, K.; Truflandier, L. A.; Brendler, E.; Wagler, J. *Chem. Eur. J.* **2012**, *18*, 12803-12813. (n) Wächtler, E.; Gericke, R.; Zhechkov, L.; Heine, T.; Langer, T.; Gerke, B.; Pöttgen, R.; Wagler, J. *Chem. Commun.* **2014**, *50*, 5382-5384. (o) Wahlicht, S.; Brendler, E.; Heine, T.; Zhechkov, L.; Wagler, J. *Organometallics* **2014**, *33*, 2479-2488. (p) Kameo, H.; Kawamoto, T.; Bourissou, D.; Sakaki, S.; Nakazawa, H. *Organometallics* **2015**, *34,* 1440-1448. (q) Gualco, P.; Ladeira, S.; Kameo, H.; Nakazawa, H.; Mercy, M.; Maron, L.; Amgoune, A.; Bourissou, D. *Organometallics* **2015**, *34*, 1449-1453. (r) Sun, J.; Ou, C.; Wang, C.; Uchiyama, M.; Deng, L. *Organometallics* **2015**, *34*, 1546-1551. (s) Krebs, K.

M.; Freitag, S.; Schubert, H.; Gerke, B.; Pöttgen, R.; Wesemann, L. *Chem. Eur. J.*, **2015**, *21*, 4628-4638. (t) Lin, T.-P.; Gabbai, F. P. *Polyhedron* **2017**, *125*, 18-25.

(25) (a) Tse, J. S.; Lee, F. L.; Gabe, E. J. *Acta Crystallogr. Sect. C* **1986**, *42*, 1876. (b) Ng, S. W. *Acta Crystallogr. Sect. C* **1995**, *51*, 2292.

(26) Analysis of charge-transfer (CT) energy was performed using the second-order perturbation with the NBOs.

(27) (a) Vosko, S.H.; Wilk, L.; Nusair, M. *Can. J. Phys.* **1980**, *58*, 1200-1211. (b) Becke, A.D. *Phys. Rev.* **1988**, *A38*, 3098-3100. (c) Becke, A.D. *J. Chem. Phys.* **1993**, *98*, 5648-5652. (d) Perdew, J.P.; Wang, Y. *Phys. Rev.* **1992**, *B45*, 13244-13249.

(28) Wilkinson, G. *Inorg. Synth.* **1972**, *13*, 126.

(29) The influence of the borane coordination on the electron density of transition metal centers were similarly discussed using CO frequency; see (a) Bontemps, S.; Sircoglou, M.; Bouhadir, G.; Puschmann, H.; Howard, J. A. K.; Dyer, P. W.; Miqueu, K.; Bourissou, D. *Chem. Eur. J.* **2008**, *14*, 731-740. (b) Gualco, P.; Mercy, M.; Ladeira, S.; Maron, L.; Amgoune, A.; Bourissou, D. *Chem. Eur. J.* **2010**, *16*, 10808-10817. (c) Kameo, H.;

Hashimoto, Y.; Nakazawa, H. *Organometallics* **2012**, *31*, 3155-3162.

(30) One of two independent molecules is displayed here, and the other molecule is shown on page S12 in Supporting Information.

(31) In the solid state, the Si center in **9-BF$_4$**, was separated more than 5.0 Å from the BF_4 anion.

(32) Calculations on the real system (without replacement) were also performed on Sn-F bond activation, which basically provides similar results to model system; see page S19 in Supporting Information.

(33) PPh_3 may contribute to promoting the proton loss, which is not very clear at this stage.

(34) Kutzelnigg, W. *Angew. Chem. Int. Ed. Engl.* **1984**, *23*, 272-295.

(35) Five membered-rings E-C_{ipso}-C_{ipso}-P-Ir change in the bond activation processes (the conversion from **A1^E** (E = Si, Sn) to **A2^E** (E = Si, Sn)) as shown follows (Average of three distances and angles are given). The geometrical changes are smaller in Sn than in Si systems, predicting that the stabilization by geometrical changes would be smaller in Sn

system.

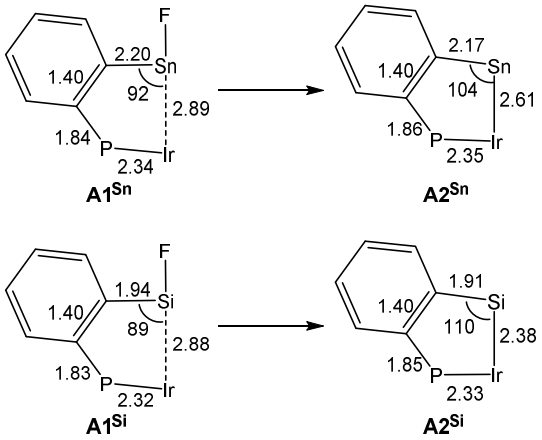

(36) Selected examples for Sn−Cl bond activation by late transition metals: (*a*) Kuyper, J. *Inorg. Chem.* **1978**, *17*, 77-81. (b) Kuyper, J. *Inorg. Chem.* **1978**, *16*, 2171-2176. (c) Levy, C. J.; Vittal, J. J.; Puddephatt, R. J. *Organometallics* **1996**, *15*, 2108-2117. (d) Levy, C. J.; Puddephatt, R. J. *J. Am. Chem. Soc*. **1997**, *119*, 10127-10136. (e) Rendina, L.M.; Puddephatt, R.J. *Chem. Rev.* **1997**, *97*, 1735-1754. (f) Janzen C. R.; Jennings, M. C.; Puddephatt, R. J. *Organometallics* **2001**, *20*, 4100-4106. (g) Cabon, Y.; Reboule, I.; Lutz, M.; Gebbink, R. J. M. K.; Deelman, B.-J. *Organometallics* **2010**, *29*, 5904-5911. (h) Warsink, S.; Derrah, E. J.; Boon, C. A.; Cabon, Y.; de Pater, J. J. M.; Lutz, M.; Gebbink, R. J. M. K.; Deelman, B.-J. *Chem. Eur. J.* **2015**, *21*, 1765–1779. (i) Wächtler, E.; Wahlicht, S.; Privér, S. H.; Bennett, M. A.; Gerke, B.; Pöttgen, R.; Brendler, E.; Gericke, R.; Wagler, J.;

Bhargava, S. K. *Inorg. Chem.* **2017**, *56*, 5316-5327.

(37) (a) Wade, C. R.; Gabbaï, F. P. *Angew. Chem. Int. Ed.* **2011**, *50*, 7369-7372. (b) Wade, C. R.; Ke, I.-S.; Gabbaï, F. P. *Angew. Chem. Int. Ed.* **2012**, *51*, 478-481. (c) Ke, I.-S.; Gabbaï, F. P. *Inorg. Chem.*, **2013**, *52*, 7145-7151. (d) Ke, I.-S.; Jones, J. S.; Gabbaï, F. P. *Angew. Chem. Int. Ed.* **2014**, *53*, 2633-2637. (e) Jones, J. S.; Wade, C. R.; Gabbaï, F. P. *Angew. Chem. Int. Ed.* **2014**, *53*, 8876-8879. (f) Jones, J. S.; Gabbaï, F. P. *Acc. Chem. Res.* **2016**, *49*, 857-867.

(38) Although DFT calculations provided fairly plausible pathways for Sn−X bond cleavage (X = F, Cl), the possibility of bimolecular (intermolecular) mechanism at Sn−X bond cleavage step could not be ruled out.

(39) Rigaku. REQAB. Version 1.1. Rigaku Coporation, Tokyo, Japan, 1998.

(40) Altomare, A.; Burla, M.C.; Camalli, M.; Cascarano, G.; Giacovazzo, C.; Guagliard, A.; Moliterni, A.G.G.; Spagna, R. *J. Appl. Crystallogr.* **1999**, *32*, 115.

(38) G.M. Sheldrick, SHELXL97: Program for the Refinement of Crystal Structures, University of Göttingen, Germany, 1997.

(39) Frisch, M. J.; Trucks, G. W.; Schlegel, H. B.; Scuseria, G. E.; Robb, M. A.; Cheeseman, J. R.; Scalmani, G.; Barone, V.; Mennucci, B.; Petersson, G. A.; Nakatsuji, H.; Caricato, M.; Li, X.; Hratchian, H. P.; Izmaylov, A. F.; Bloino, J.; Zheng, G.; Sonnenberg, J. L.; Hada, M.; Ehara, M.; Toyota, K.; Fukuda, R.; Hasegawa, J.; Ishida, M.; Nakajima, T.; Honda, Y.; Kitao, O.; Nakai, H.; Vreven, T.; Montgomery, Jr., J. A.; Peralta, J. E.; Ogliaro, F.; Bearpark, M.; Heyd, J. J.; Brothers, E.; Kudin, K. N.; Staroverov, V. N.; Kobayashi, R.; Normand, J.; Raghavachari, K.; Rendell, A.; Burant, J. C.; Iyengar, S. S.; Tomasi, J.; Cossi, M.; Rega, N.; Millam, N. J.; Klene, M.; Knox, J. E.; Cross, J. B.; Bakken, V.; Adamo, C.; Jaramillo, J.; Gomperts, R.; Stratmann, R. E.; Yazyev, O.; Austin, A. J.; Cammi, R.; Pomelli, C.; Ochterski, J. W.; Martin, R. L.; Morokuma, K.; Zakrzewski, V. G.; Voth, G. A.; Salvador, P.; Dannenberg, J. J.; Dapprich, S.; Daniels, A. D.; Farkas, Ö.; Foresman, J. B.; Ortiz, J. V.; Cioslowski, J.; Fox, D. J. *Gaussian09*, Gaussian, Inc., Wallingford CT, **2009**.

(40) (a) Mennucci, B.; Tomasi, J. *J. Chem. Phys.* **1997**, *106*, 5151-5198. (b) Cancés, M.T.; Mennucci, B. J.; Tomasi, J. *J. Chem. Phys*, **1997**, *107*, 3032-3041. (c) Cossi, M.; Barone, V.; Mennucci, B.; Tomasi, J. *Chem. Phys. Lett*, **1998**, *286*, 253-260. (d) Tomasi, J.; Persico, M. *Chem. Rev.* **1994**, *94*, 2027-2094.

(41) (a) Andrae, D.; Haeussermann, U.; Dolg, M.; Stoll, H.; Preuss, H. *Theor. Chem. Acc.*, **1990**, *77*, 123-141. (b) Bergner, A.; Dolg, M.; Kuechle, W.; Stoll, H.; Preuss, H. "Ab-initio energy-adjusted pseudopotentials for elements of groups 13-17," *Mol. Phys.*, **1993**, *80*, 1431-1441.

(42) (a) Krishnan, R.; Binkley, J.S.; Seeger, R.; Pople, J.A. *J. Chem. Phys.* **1980**, *72*, 650-654. (b) McLean, A.D.; Chandler, G.S. *J. Chem. Phys.* **1980**, *72*, 5639-5648.

(43) Yawari, P. S.; Reddy A.; Strivastava, M, A. *RSC Adv.* **2013**, *3*, 17244-17253.

Graphical abstract